DYNAMIC EFFECTS OF HIGH ν/γ BEAM PLASMA INTERACTIONS

PITR-106-1

by

Gerold Yonas, Philip Spence, Don Pellinen,
Bruce Ecker, and Sergei Heurlin

April 1969

Prepared for

Defense Atomic Support Agency
Washington, D. C. 20305

This research is being sponsored
by the Defense Atomic Support Agency
under Contract DASA-01-68-C-0096

Physics International Company
2700 Merced Street
San Leandro, California 94577

CONTENTS

ILLUSTRATIONS

ILLUSTRATIONS (cont.)

ABSTRACT

Time and spatial definition of high ν/γ beam generation and propagation has been investigated using calorimetry, voltage and current diagnostics and time of flight measurements. This work demonstrates that the main portion of these beams, in 0.5 to 1.0 torr air, propagates with a value of $(\nu/\gamma)_{net}$ which is approximately 1.0 and roughly equal values of energy in the longitudinal and transverse components of motion. The beam front propagates at velocities considerably slower than the main portion of the beam and work done by the induced electric field, due to the initial current rise, contributes to energy loss. Time-dependent measurements of net and primary current have been correlated with a diffusion dominated model of current neutralization, the key parameters in this model being the risetime of the primary current, the avalanche breakdown time of the gas, and the plasma conductivity after breakdown. Beam manipulation experiments, such as shaping, splitting and recombination, and attempts to form an electron ring are also reported.

FOREWORD

This report presents the interim results of work on a continuing high ν/γ beam physics program, and covers the period from November 1, 1968 to March 15, 1969. The program is supported by DASA contract No. DASA-01-68-C-0096 and is monitored by Lt. J. M. Wachtel. The goals of the program are the definition of the time dependence of diode impedance on diode geometry, the determination of the primary beam and plasma currents, the study of high ν/γ beam transport efficiency and time of flight, and the investigation of various beam control and manipulation techniques. The work was conducted by members of Physics International Company's Vulnerability Department, under the supervision of Dr. Alan Klein. Principal investigators were Dr. Gerold Yonas, Program Manager; Dr. Philip Spence, Physicist; Donald Pellinen, diagnostics development; Bruce Ecker and Sergei Heurlin, data collection and reduction. Sidney Putnam and John Creedon contributed to the program through numerous helpful discussions.

SECTION I

INTRODUCTION

Experimental investigations of high ν/γ electron beams, documented in DASA 2175 (Reference 1) were directed toward uncovering basic phenomenological aspects of beam transport. From this study it became clear that current neutralization was essential in efficiently transporting high ν/γ beams over appreciable distances, and that an optimum pressure range existed for air (0.5 - 1.0 torr). The major diagnostic tools consisted of calorimetry and open shutter photographs, although preliminary work was conducted with voltage and current probes and a B-field probe in the drift chamber. Measurements of net currents using a single loop off axis indicated peak net currents of approximately 2 to 3 kA in the 0.5 - 1.0 torr pressure range (see Figures 29-31, Reference 1). Considerable oscillations were apparent throughout the pulse, and this structure was poorly understood (Figure 32, Reference 1).

It was found, however, that beams guided and transported in small-diameter conducting pipes yield more straight forward measurements of net and primary currents. It was also decided to more fully investigate the diode diagnostics to accurately define the initial electron energy spectrum. Although the voltage and current monitors had given fair correlation with measured deposition profiles (Figure 18, Reference 1), a correction had not been made for the inductive signal measured with the diode shorted. The impedance based on average voltage and current (which had indicated a Child's Law dependence) had been gathered only for a limited range of anode-cathode spacings.

The primary goals of this work were, then, to better determine the spatial and time dependence of primary and secondary currents, and to define the time dependence of the accelerating voltage and tube current. Other questions have been raised relative to the modeling of electron trajectories, and time of flight measurements were suggested to provide a measurement of beam transverse energy.

This program began with a careful check of previous calibration techniques and the development of (1) a low-inductance, resistive, wall current monitor, (2) a self-integrating Rogowski coil to be placed in a slot in the guide tube wall, and (3) a Faraday cup capable of measuring 100 kA primary beam currents (electron energies of approximately 200 keV).

The conclusions to date can be summarized as follows:

1. Diode voltage and current have been measured for several anode-cathode distances, (A-K), corrected for the inductive component, and used to generate energy spectra, deposition profiles, and total beam energy. A detailed picture of the time dependence of the diode impedance as a function of (A-K) has been obtained. The most important features are that the diode impedance tends to decrease throughout the pulse for high ν/γ, and to be more stable for ν/γ closer to 1.0, and that comparison with Child's Law based on average values, avoids the inherent complexity of the process.

2. Propagation velocities of the beam front and interior have been determined with a scintillator/photo-diode measurement of the bremsstrahlung produced by a target at the ends of pipes of various lengths, at several pressures. The conclusion was that the beam front slows down with distance and has the largest transport velocity at approximately 1.0 torr. Interior portions

of the beam travel at higher velocities than the front, but their velocity is lower than that predicted by diode measurements of spectra. The slowing down of the front has been interpreted in terms of work done by the longitudinal electric field near the front. The lower transport velocities for the majority of the beam electrons are considered to be a result of a transverse velocity component. Measurements of $(\nu/\gamma)_{net}$ using the Rogowski coils and wall shunts support the conclusion that transverse components of velocity are significant.

3. By measuring the net current with a wall shunt or Rogowski coil recessed into the wall, it was possible to define the actual degree of current neutralization immediately adjacent to the beam channel. The geometry is well defined, and any back current flowing outside the primary beam channel, thought to have been the case in previous measurements, is not included in the net current measurement.

Net current was measured in air, argon, and helium in various length pipes at several pressures. We deduced that the avalanche breakdown of the gas in the initial longitudinal electric field governed the magnitude of net current early in the pulse, and that net currents giving $(\nu/\gamma)_{net} \sim 0.5 - 1.0$ occurred late in the pulse. This indication supports the conclusion, based on beam timing, that the electron trajectories are not straight, but does not indicate any substantial deviation from a Lawson model interpretation.

4. The time dependence of the primary current was measured directly at the end of a pipe of a given length, yielding several interesting observations. Using the primary current data and a simple model of current neutralization, we have suggested an

explanation of the net current time dependence. Also, by comparing measured electron transmission through filters of various thickness with Monte Carlo calculations, we obtained information on the average incident electron angle on a plane normal to the guide pipe exit. At 0.5 torr, non-zero average electron angles were found at the exit of the shallow angle guide cone. With a Rogowski coil at the cone exit it was simultaneously determined that $\nu/\gamma_{net} \sim 1.0$. Preliminary measurements indicated that angles in the 30-60 deg range are possible.

5. It was demonstrated that beams can be split into two or more separate beams by inserting a sharp edged plane in a pipe. Attempts to recombine beams have been inconclusive. Initial experiments to reinject a beam into its wake indicate that some care must be exercised in the manner of injection, and that energy loss is caused by propagation past the discontinuity at the reinjection point. These and other speculative experiments were generally de-emphasized in favor of utilizing the diagnostic tools recently developed.

SECTION II

DIODE BEHAVIOR

A. VOLTAGE AND CURRENT DIAGNOSTICS

In recent months the diode diagnostics on the Model 730 Pulserad have been upgraded to more accurately determine the time dependence of the electron energy spectrum. The diode voltage monitor described in DASA 2175 was modified at its bottom stage for use at cathode voltages up to 500 kV. Other improvements include a more sturdy magnetic shield and a dial gauge to measure anode-cathode spacing when the diode is pumped down to typical operating pressures.

The monitors were checked out by the following series of experiments:

1. The diode current monitor was calibrated by firing the beam into a Faraday cup located at the anode plane at both high (200 kA) and low (50 kA) current levels. The diode voltage monitor was calibrated at 25 kV with an external voltage source.

2. After the magnetic shield was installed, the inductive pickup of the voltage monitor (Figure 1c) was measured for anode-cathode shorted shots and correlated with the signal from a separate $\partial B/\partial t$ probe located in the diode region. The $\partial B/\partial t$ probe was then used as a measure of the inductive component of the diode voltage signal on all subsequent shots. This component was subtracted from the voltage monitor signal (Figure 1d) to yield the actual accelerating voltage pulse shape (Figure 1e).

3. A series of low-current, $(v/\gamma)_{primary} \sim 1.6$, shots were taken with graphite and thin foil calorimeters placed 2-3 cm from

the anode plane. At high ν/γ, large current densities at the anode, which cause catastrophic damage to the calorimeters, preclude this experiment. The total beam energy was observed to agree (± 5%) with $\int_0^\infty V \cdot I \, dt$ calculated from voltage and current records.

4. The pulser was fired at normal current levels and at mean voltage levels of 500, 400, 300, and 200 kV (ν/γ = 7, 8, 9.6, and 12). Energy deposition profiles agreed with calculations based on voltage and current monitor data at the higher mean electron energies (Figures 2, 3, and 4).* At approximately 200 keV the calculated deposition profile was less peaked near the front surface of the target than was typically measured (see Figure 5). Simultaneous measurements of net beam currents and beam transmission through thin foils suggest transverse energy components in the 200-keV beam; this would result in an energy deposition profile consistant with the measured current and voltage spectrum and average angles of incidence of $\theta \sim 45^\circ$ at the target. (This is discussed in Section III.)

B. TIME DEPENDENCE OF DIODE IMPEDANCE

After checking previous techniques of calibrating the voltage and current monitors, measuring anode-cathode distances, and correcting for the inductive component of tube voltage signal, we looked again at the question of diode impedance. Based on a limited range of anode-cathode distances and relying heavily on deposition profiles to give mean electron energies, we concluded in DASA 2175 that the average impedance, defined there as $\langle V \rangle / \langle I \rangle$, could be described in terms of a Child's law dependance,

$$\frac{\langle V \rangle}{\langle I \rangle} = \frac{K}{\langle V \rangle^{1/2}} \frac{d^2}{r^2}$$

*Replications of the deposition profile measurements at 400-500 keV show a deposition near the front surface which more closely matches the calculations; Figures 2 and 3 are not typical in view of recent data.

<E> = 0.524 MeV

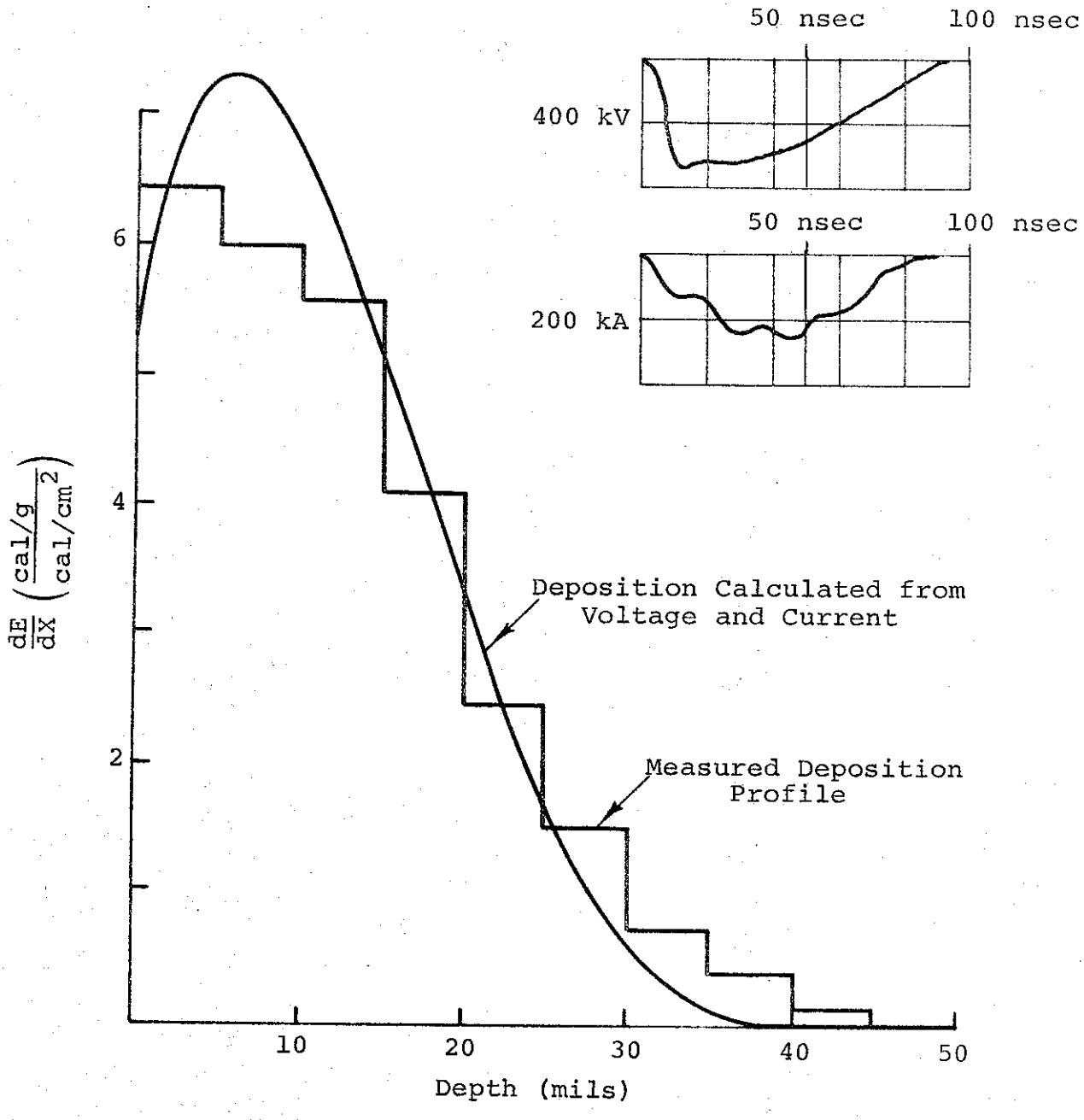

FIGURE 2. MEASURED AND CALCULATED DISPOSITION PROFILES--<E> = 0.524 MeV

5799

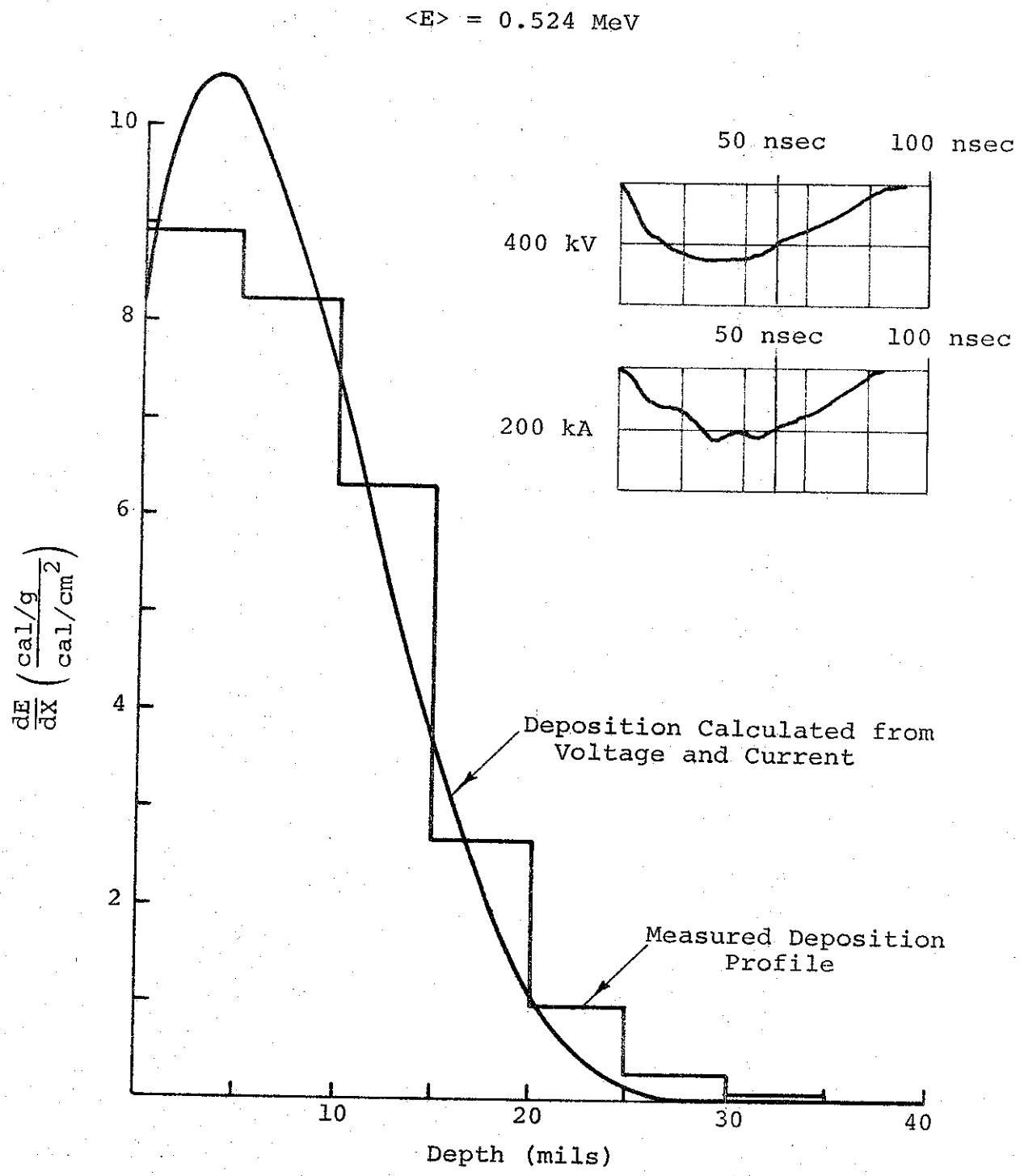

FIGURE 3. MEASURED AND CALCULATED DISPOSITION PROFILES--<E> = 0.397 MeV

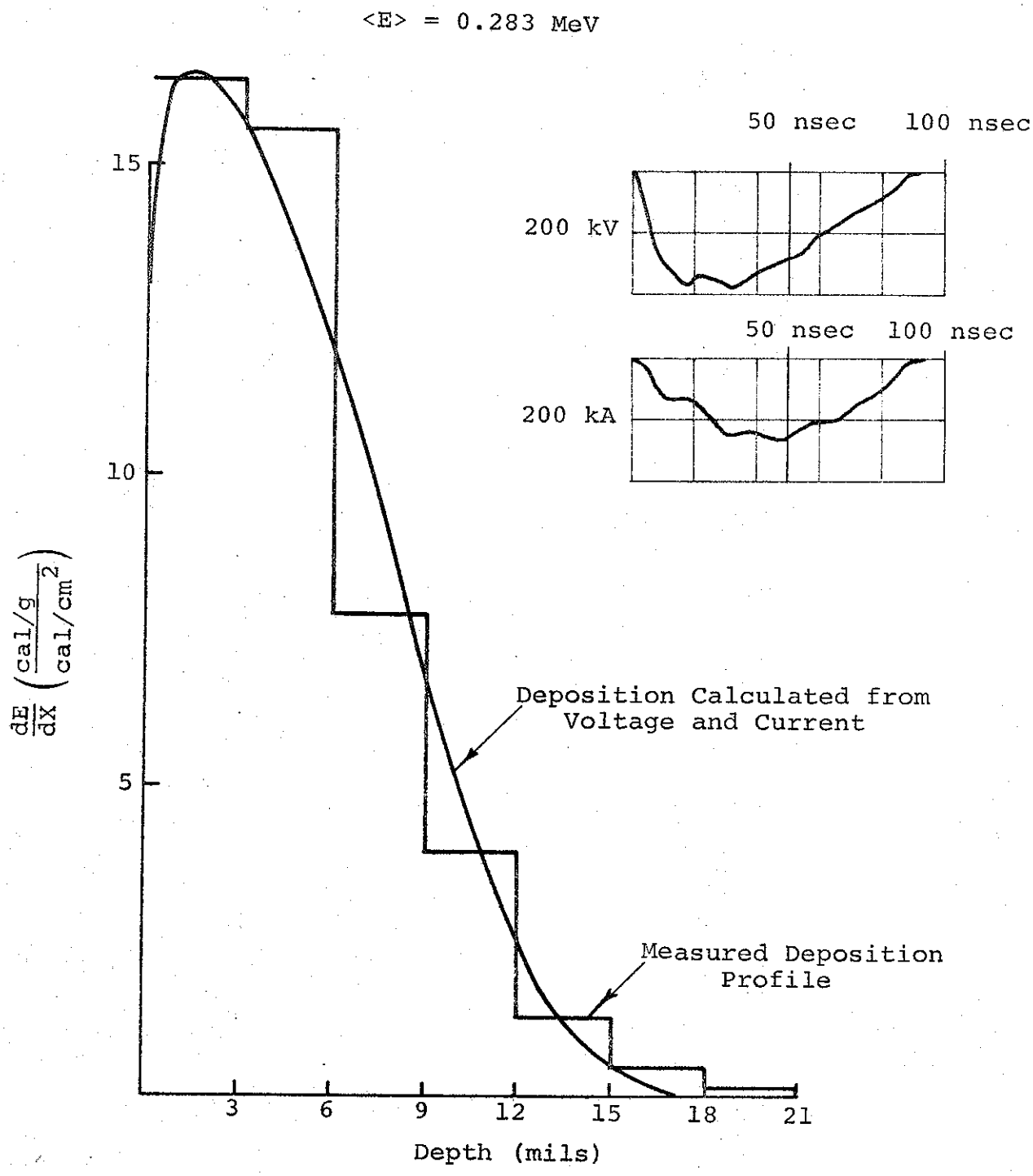

FIGURE 4. MEASURED AND CALCULATED DISPOSITION PROFILES--<E> = 0.283 MeV

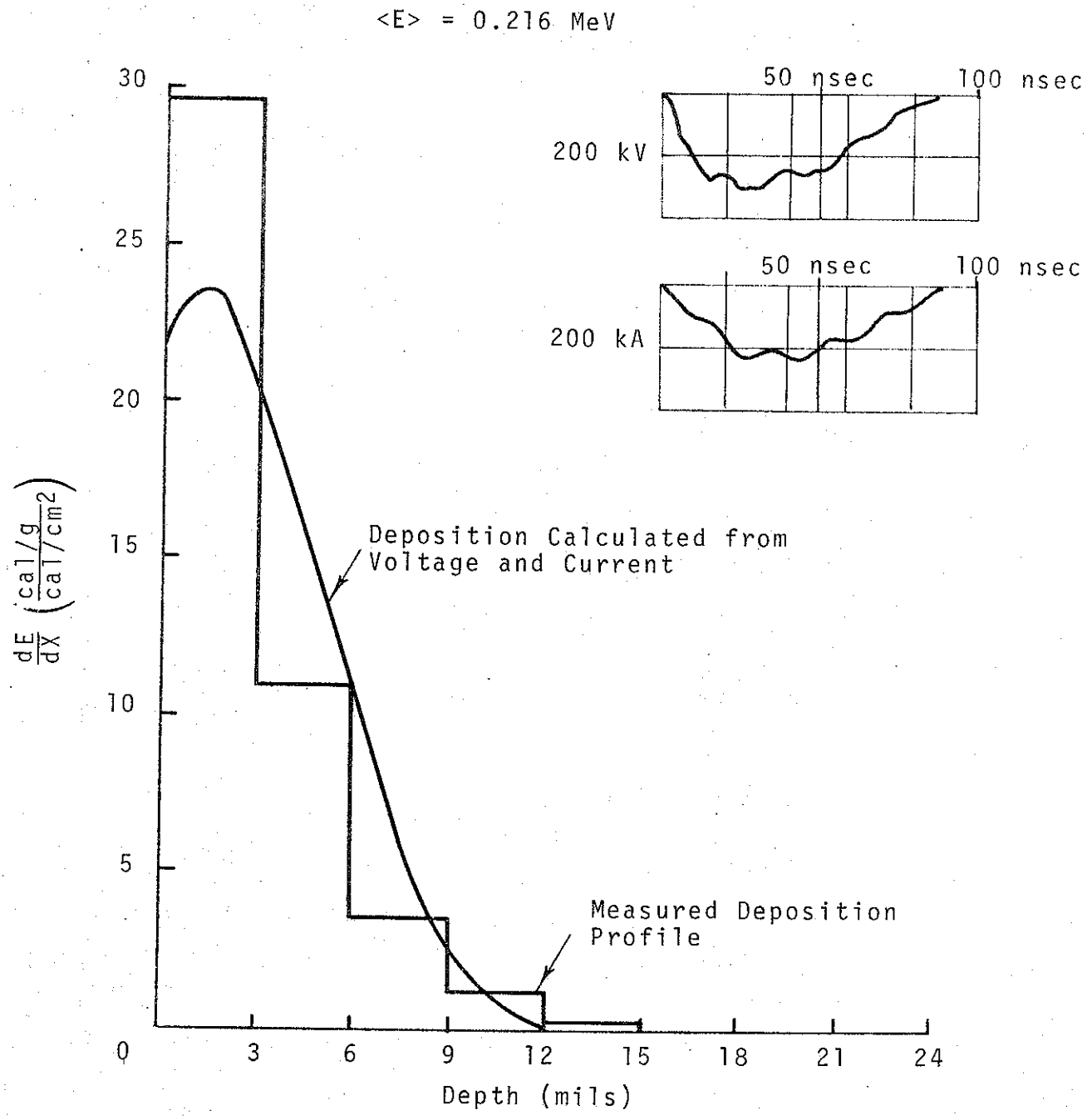

FIGURE 5. MEASURED AND CALCULATED DEPOSITION PROFILES--<E> = 0.216 MeV

We reported that the data could be correlated with a value of $K = 115$ (impedance in Ω; V in MV), assuming plane parallel space charge limited flow from a circular disk cathode of radius $r = 3.2$ cm.

Recent work based on these more complete diagnostics has provided a more accurate estimate of the average impedance, but more important, has shown that the diode impedance is a far more complex function of anode-cathode distance and time than previously implied.

Figure 6 gives the diode impedance (V/I) as a function of time; generally, the impedance appears to drop rapidly early in the pulse but tends to remain more constant through the pulse for ν/γ closer to one than for the high ν/γ cases (see Figure 7). Calculating K as a function of time, we obtain the results shown in Figure 8. Late in the pulse, the impedance roughly agrees with ~ 1/3 the Child's law impedance, but between 20 and 40 nsec into the pulse, K first increases, then decreases as the anode-cathode distance increases.

The drop in impedance late in the pulse is probably explained by plasma formation from both cathode and anode material, but a detailed understanding of the behavior early in the pulse would require a solution of the time dependent trajectory problem. It appears that such an analysis will be required to fully understand these results and predict diode characteristics at even higher values of ν/γ.

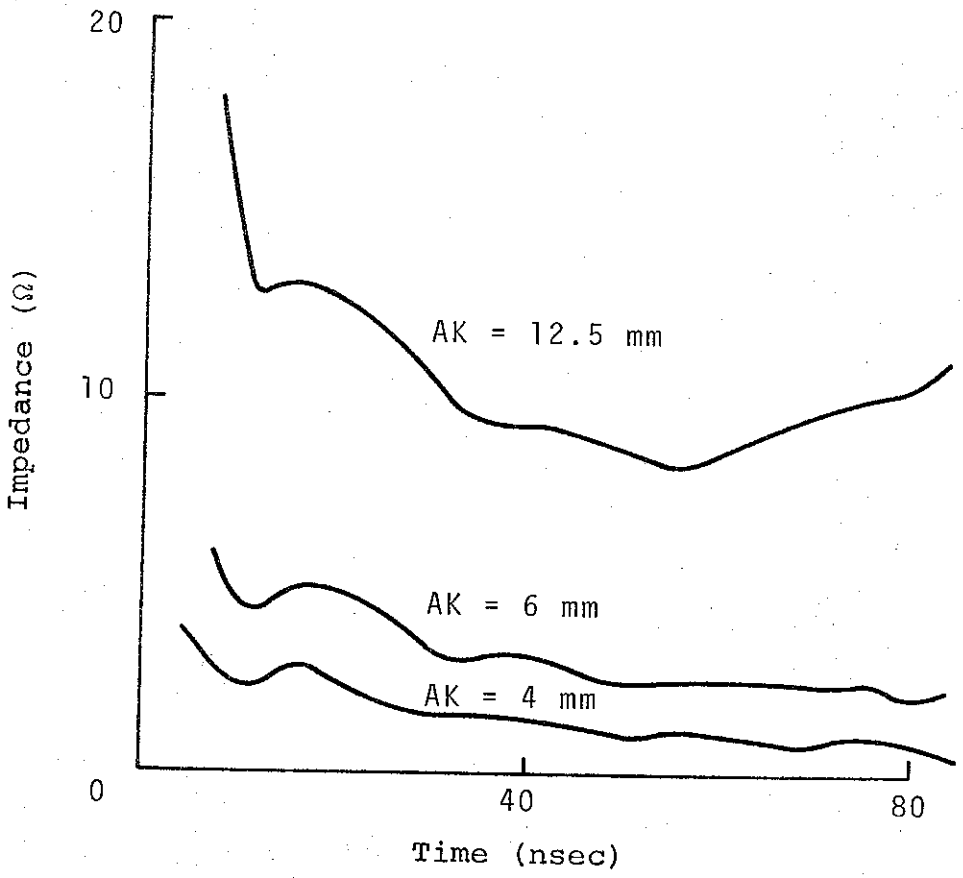

FIGURE 6. DIODE IMPEDANCE VERSUS TIME

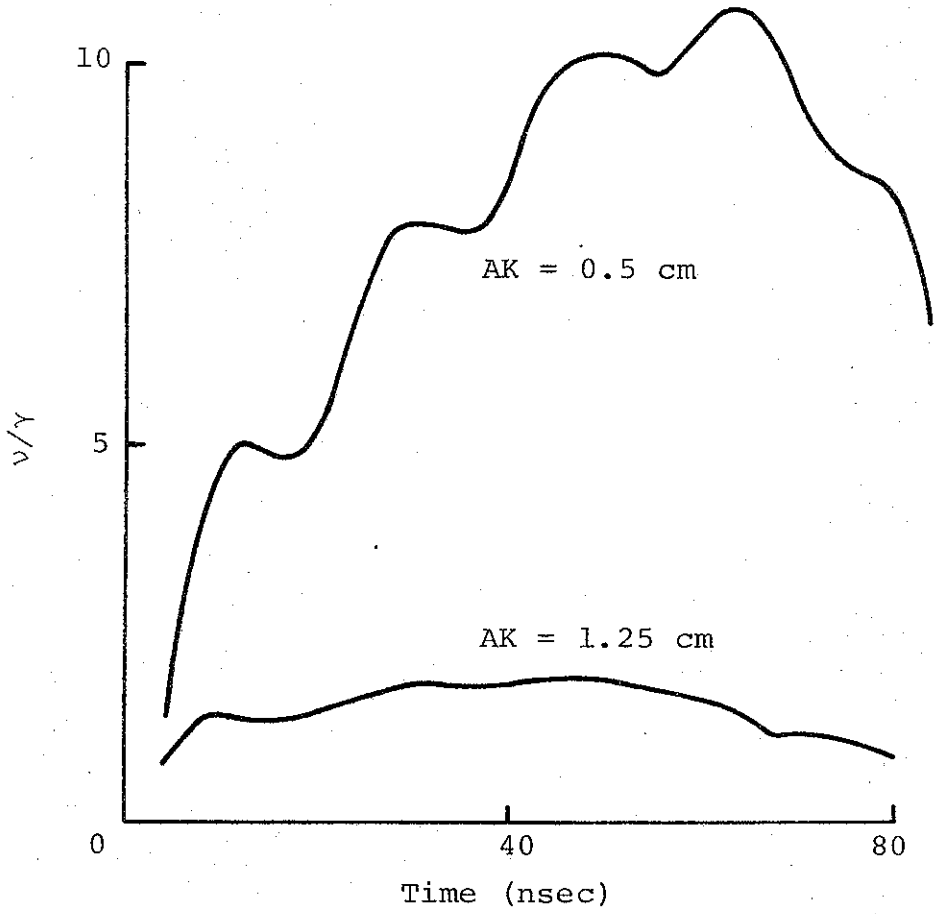

FIGURE 7. ν/γ VERSUS TIME

5794

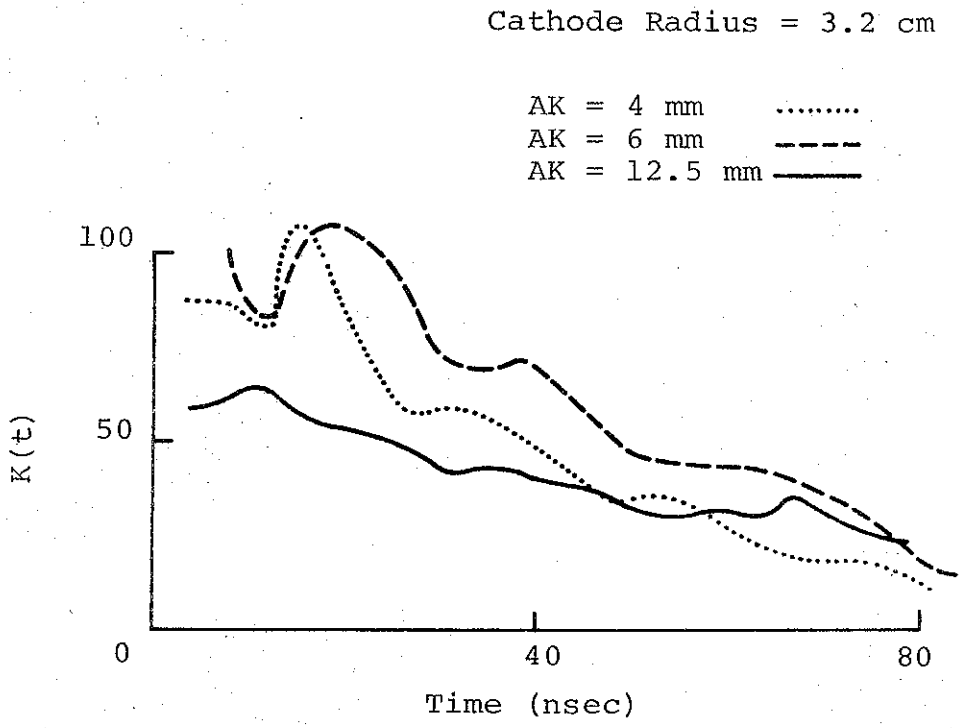

FIGURE 8. K VERSUS TIME

SECTION III

BEAM BEHAVIOR

A. DRIFT CHAMBER DIAGNOSTICS

Three new diagnostics--a self-integrating Rogowski coil, a wall current monitor, and a Faraday cup (to measure primary accelerated beam currents)--have been constructed as part of this investigation. Figure 9 shows the three monitors and the experimental configuration.

1. Rogowski Coil*

The Rogowski coil, a modification of the single-turn, self-integrating B probe used in prior experiments, has many small turns forming a loosely wound torus. The coil is self-integrating and has a voltage output proportional to the average flux threading all turns. This diagnostic measures the net current flowing through the guide pipe. A completed coil is shown in Figure 10. Neglecting any mutual inductance between the separate turns of the Rogowski coil, and assuming that the voltage drop across the monitor circuit occurs only across the integrating resistor, it can be shown that the output voltage is

$$V = \frac{R}{L}\, n\, A\, \mu_o I/2\pi a \quad \text{(mks)}$$

where

R = resistance of integrating resistor,
L = net self-inductance of the coil,
n = number of turns in coil,
A = area of a single turn,
a = mean radius of the torus.

*A Rowgowski coil is usually considered to be a coil whose output is proportional to $\partial\phi/\partial t$ rather than $\phi(t)$.

In view of the approximations involved in determining the Rogowski coil output, an empirical calibration was necessary. A calibration fixture and fast readout system have been developed from the following:

a. Fast risetime pulse generator, 10 A into 50-Ω load with a 2 nsec risetime,

b. Sampling oscilloscope, 2 mV/cm sensitivity, 0.3 nsec risetime,

c. Impedance matching load threading the coil.

The calibration fixture is shown later in Figure 13. A typical calibration trace on the sampling oscilloscope is shown in Figure 11a, where the upper trace is the coil output, and the lower is the input current pulse. Figure 11b shows the coil response to a longer (270 nsec) 10-A input pulse. A summary of the characteristics for coil No. 15 is given below. Similar calibrations were performed on all Rogowski coils constructed for this work.

COIL CHARACTERISTICS

2-cm i.d. Rogowski Coil No. 15

Risetime	0.9 nsec
Absolute Sensitivity	4.8 V/kA
Decay Constant	400 nsec

2. Wall Current Shunt

The net current measured with the Rogowski coil should equal the wall current if one requires that no appreciable amount of charge can build up at any time between two points in the pipe. Then, $\vec{I}_{pr} + \vec{I}_{pl} + \vec{I}_{w} = 0$, where $\vec{I}_{pr}$ is the primary beam current, $\vec{I}_{pl}$ is the plasma current which flows in either direction along the beam channel depending on the sign of the electric field, and $\vec{I}_{w}$ is the wall current. This relationship immediately suggests that the net current can be measured using a shunt resistor in the pipe wall. A low-inductance resistor ($L \sim 10^{-11}$ H) was constructed as shown in Figure 12a, and can be mounted anywhere along the wall in tandem with the Rogowski coil and Faraday cup.

The shunt (calibration is given in Figure 14) is directly coupled into the circuit and does not experience the overshoot or "droop" that appears in inductively coupled devices. Thus, long plasma decay times can be interpreted without correcting the output. The shunt and Rogowski coil yield independent measurements of the net current; when their results correlate the credibility of the measurement is increased.

3. Faraday Cup and Calibration of Current Diagnostics

The Faraday cup is a charge collector combined with an integral mΩ shunting resistor similar to the device used to monitor anode currents in Reference 1. The new Faraday cup, shown in Figure 12b, is improved by incorporating a faster integral vacuum pumping system and a conical collector specifically designed to intercept high-current, low-energy electron beams. The thin rubber membrane acts as a vacuum seal in front of the collector, and in principle, prevents the plasma formed in the beam channel from shorting out the current path through the monitoring resistor.

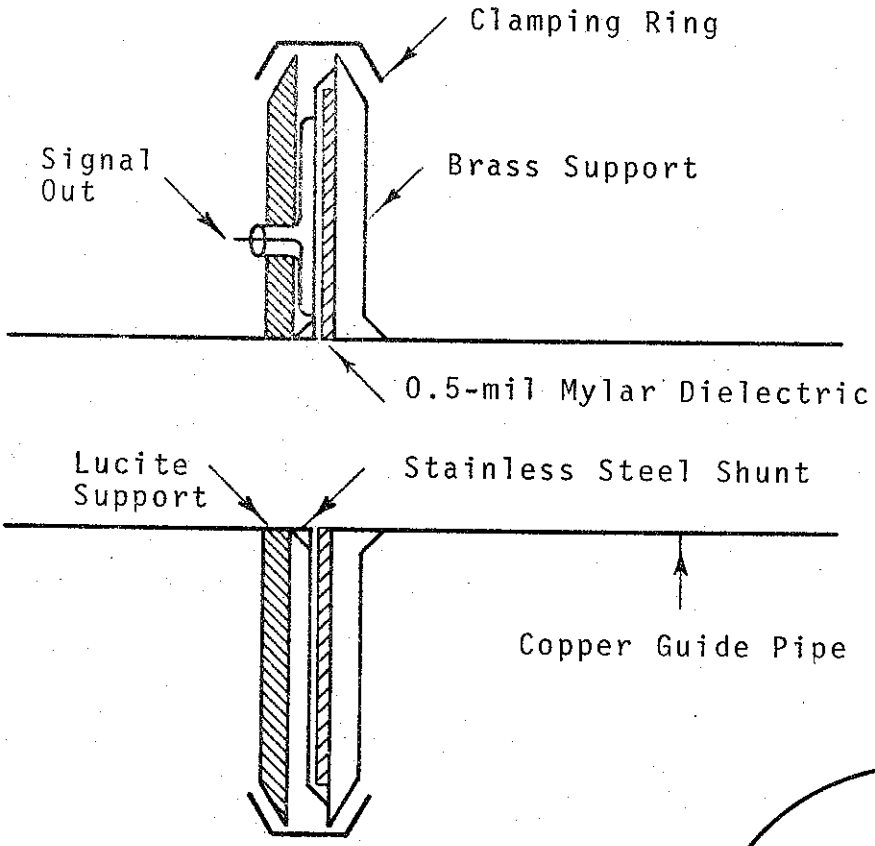

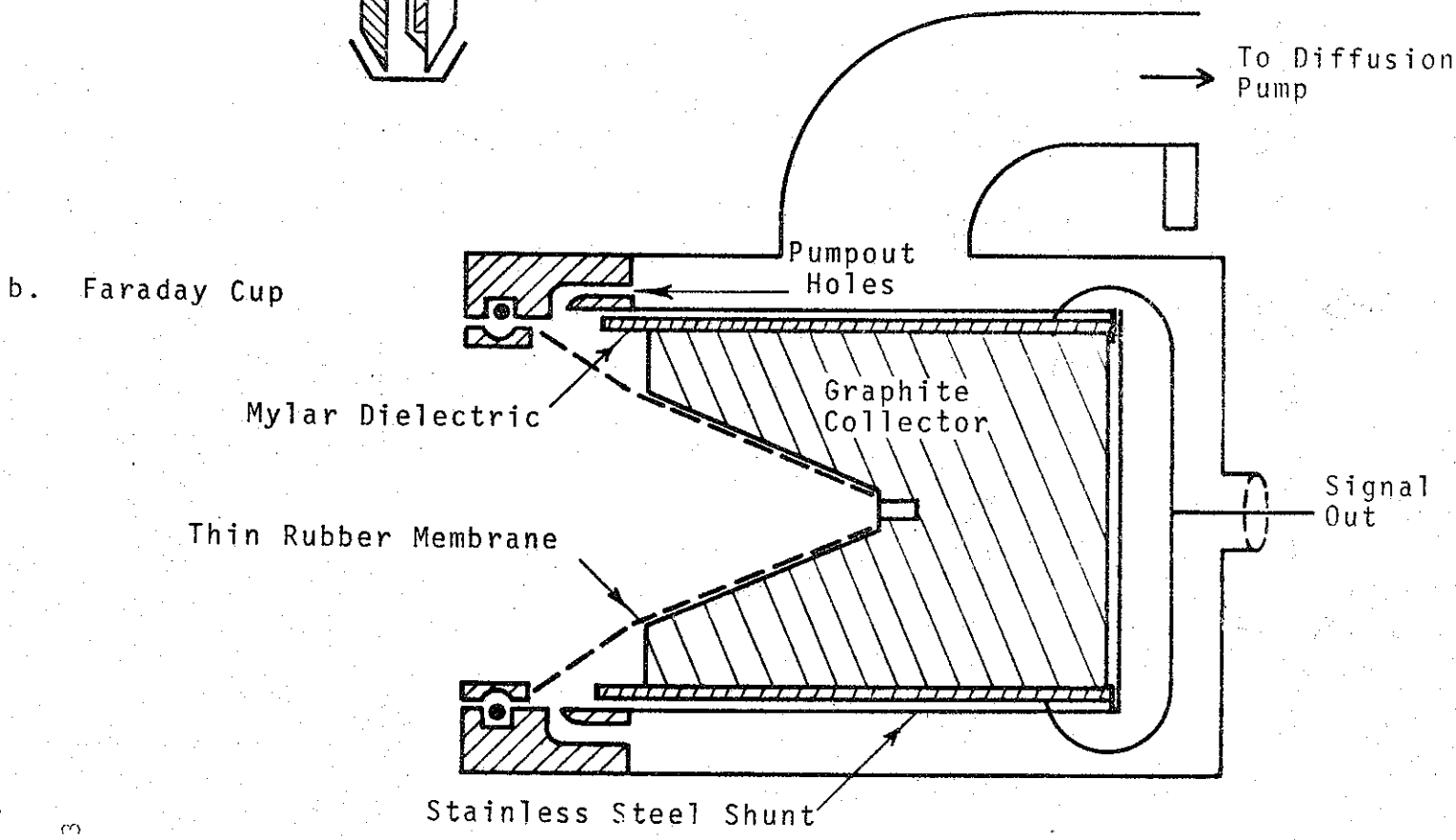

7783

FIGURE 12. SCHEMATICS OF BEAM CURRENT DIAGNOSTICS

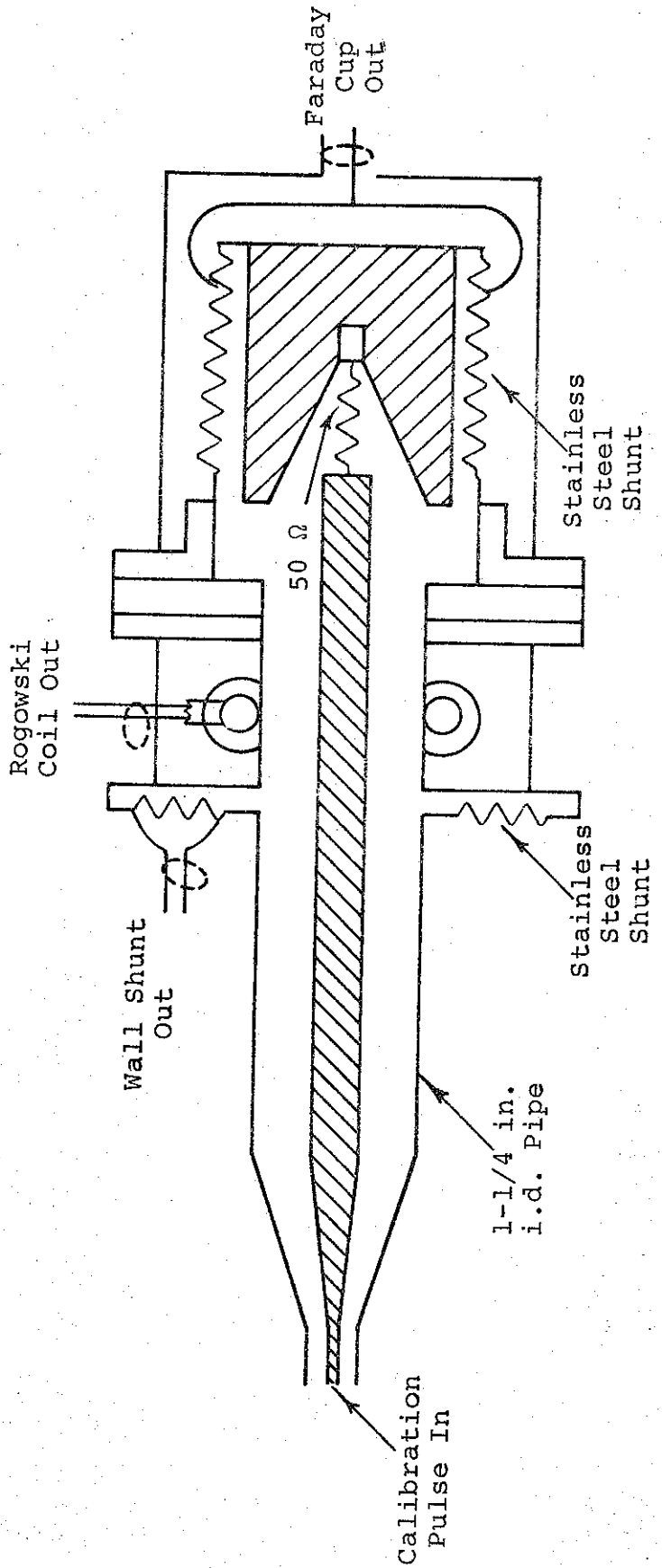

FIGURE 13. CALIBRATION FIXTURE

5798

The current incident upon the collector consists of a primary electron current, which we wish to measure, and a plasma current consisting of secondary electrons. To separate the primary electrons from the secondary charge carriers, we take advantage of the higher energy of the primary electrons and allow them to pass through a membrane which provides negligible attenuation for the primary beam but will completely stop the low-energy, secondary electrons.

When the primary electrons are injected into the evacuated space, a conservative electric field is induced by the space charge, and a nonconservative field is induced by the changing current. Calculations for simple models, such as a planar collector with a uniform charge density in the evacuated volume, indicate that the potential well generated would probably exceed the kinetic energy of the electrons, if the thickness of the evacuated region is > 2 mm.

A radial field is also induced which would tend to drive the electrons away from the collector. For a planar region of thickness Z_o with uniform charge density, ρ, the potential in the evacuated region is given by

$$V(Z) = - \rho/\varepsilon_o \ (Z_o Z - Z^2)$$

It is clear from this expression that for the beam to reach the collector, both the current density and the collector-membrane spacing must be minimized.

The conical collector was chosen to maximize the collector area and to support the membrane with a reproducible small spacing. Also, since tangential fields are produced, the probability of electron collection is enhanced. Another advantage, the space charge potential produces a field which prevents low-energy

secondary electrons from leaving the collector. An electron cannot traverse the potential well unless its energy exceeds the well depth; therefore the beam space charge should prevent secondary electrons from traversing the space.

The three monitors were simultaneously calibrated in the configuration used in the experiments. The guide pipe was used as the outer conductor of a 50-Ω coaxial line with a tapered transition piece from a GR 874 connector to the pipe designed to minimize reflections. The inner conductor had an integral termination. The entire calibration fixture is shown in Figure 13. A 10-A pulser with a 0.2-nsec risetime was the current source, and the detector output was monitored with the sampling oscilloscope (0.3 nsec risetime). A set of output traces from the Faraday cup, shunt, and 3.2-cm-i.d. Rogowski coil are shown in Figure 14, for a 10-A, 270-nsec current pulse. Note the time constant on the 3.2-cm coil is approximately 1.1 μsec. Net current decay times quoted in this report were determined from the wall current shunt data to avoid correction for the L/R decay time inherent in the Rogowski coil output.

B. PRIMARY AND NET CURRENT BEHAVIOR

1. General Discussion

Recent time-resolved measurements of net and primary beam current explain some general features of beam behavior. In these new measurements, the drift chamber diameter was sufficiently small that the primary beam current tended to fill the pipe (1-1/4-in. diam). As a result, the questions of return plasma currents have been simplified over the situation described in Reference 1. Specifically, a large plasma current which flows outside of the primary beam channel and still remains between the B-probe and the beam itself, can no longer exist.

Net current behavior can be explained by a model proposed by Creedon, Reference 3. He describes the general dependence of beam pinching or drifting in terms of the fraction of the return current carried by the plasma. Also, he suggests that the time required for the gas to become a good conductor governs whether the return current will flow through the surrounding conductor or in the beam channel. Our recent measurements substantially verify this explanation.

Quantities such as breakdown time, current decay time, and maximum net current were determined by measuring the wall current, I_w, for air, argon, and helium, and are shown in Figures 15, 16, and 17. It is clear that the maximum net current during a pulse is a strong function of pressure with a minimum at 0.75 torr in air, 1.0 torr in argon, and $\geq$ 5 torr in helium. The breakdown time is defined by the first knee in the net current curve. The decay time for the plasma current, governed by magnetic field diffusion through the plasma, indicates the final plasma conductivity.

The breakdown times we determined are consistent with pulsed-dc breakdown data given by Felsenthal and Proud (Reference 4). With this data one should be able to predict pressures for optimum transport in any gas. Optimum efficiency of transport over large distances corresponds to maximum current neutralization, which in turn depends on both the breakdown time and final plasma conductivity. The simplified model below demonstrates that rapid breakdown and high plasma conductivity are required for maximum neutralization. Our measurements indicate that optimum energy transport in air and argon occurs at pressures corresponding to short breakdown times and long current decay times. Thus, the optimum pressures were less than those required for most rapid breakdown.

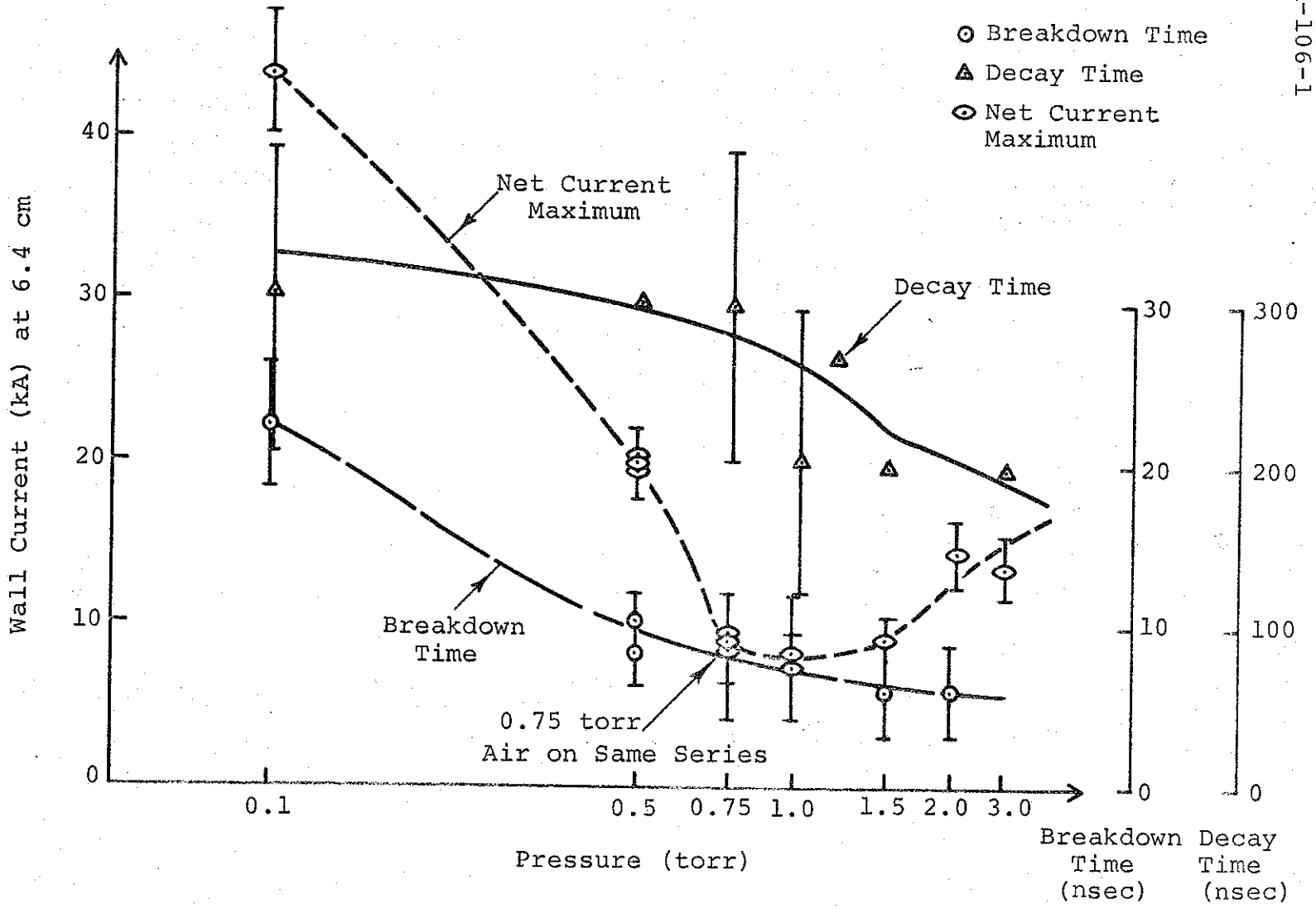

FIGURE 16. NET CURRENT, PLASMA CURRENT DECAY TIME, AND BREAKDOWN TIME VERSUS PRESSURE IN ARGON

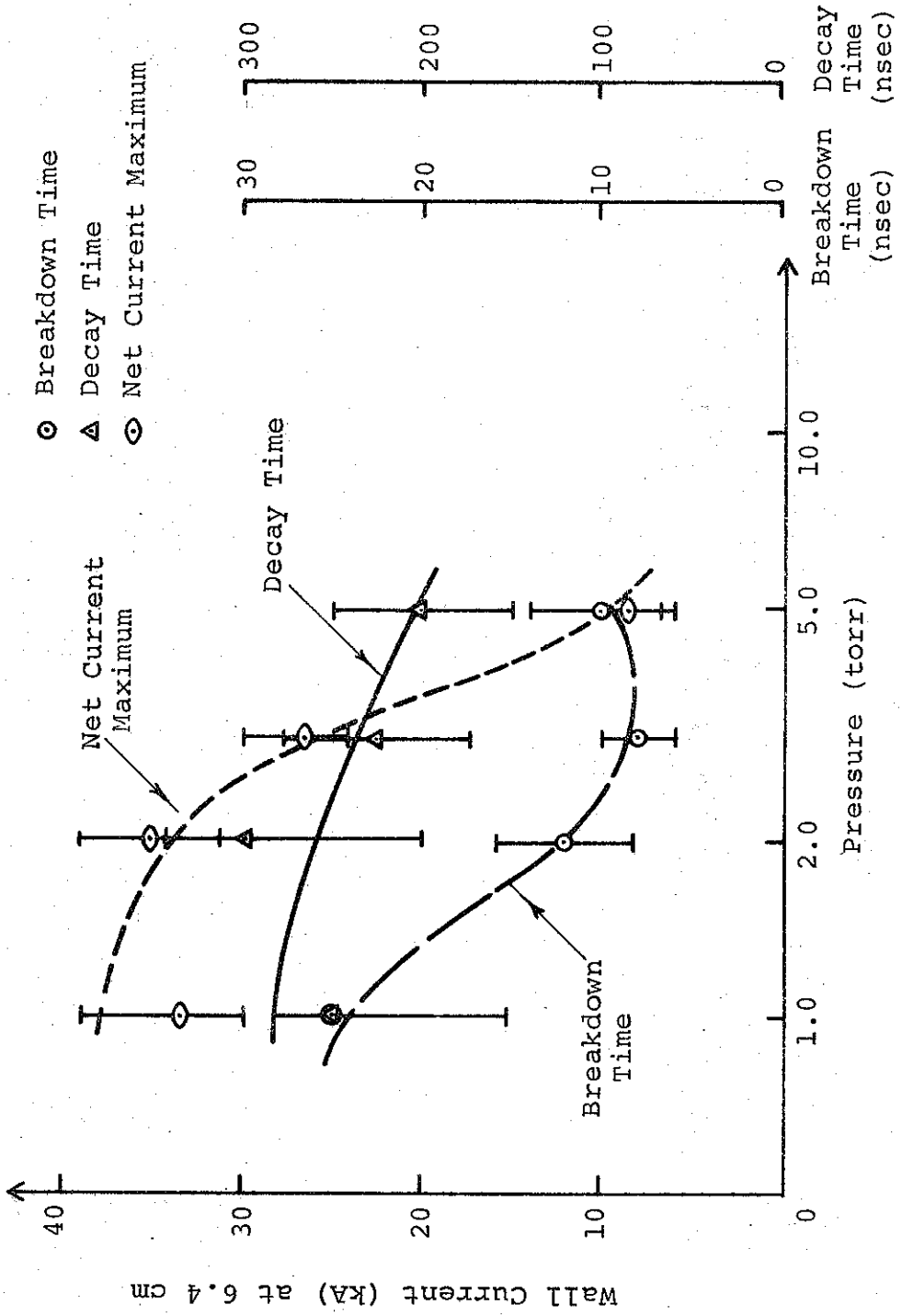

FIGURE 17. NET CURRENT, PLASMA CURRENT DECAY TIME, AND BREAKDOWN TIME VERSUS PRESSURE IN HELIUM

Other gases, such as Freon 12 which breaks down at 0.2 to 0.5 torr in approximately 4 nsec at 2000 V/cm, may yield better neutralization, but at present it seems favorable to pre-ionize the gas before injection of the electron beam. If the background gas possesses a high conductivity prior to the beam injection, current neutralization could proceed with no delay, and long-distance transport would be enhanced.

2. Time Dependence of Net Current

The initial emphasis in measurements of wall, primary, and net currents has been on determining time dependencies at the end of a 10-cm-long, 1-1/4-in.-diam pipe at pressures in the 0.5 - 1.0-torr range. The data shows net current as a strong function of breakdown time, but as expected, the risetime of the primary current exerts a strong influence on net current behavior. Our goal has been to provide a zero order relationship between the net current and the measured primary current.

Figure 18 shows net and primary currents for 0.5 and 0.75 torr. The consistent difference in the early time behavior of the primary current is readily apparent in the two cases. This difference presumably results from the coupled nature of the gas breakdown properties, the resulting plasma current, and the effect of the net current on beam guiding and transport over this short distance. Although a full analytical treatment of this problem would require a rather complex numerical scheme, we have attempted to provide an empirical model which should explain the net current behavior, given the primary current. Our first attempt utilizes several simplifying approximations. We have assumed uniform primary current over the beam width and the plasma current to be described in terms of a scalar conductivity. Segmented carbon calorimeters supported the first assumption, and the use of $(\vec{J}_{pl}) = \sigma \vec{E}$ is

valid for $\omega/\nu << 1$ (ω = electron cyclotron frequency, ν = collision frequency). With the plasma fully ionized, a decay time of ~ 100 nsec at 1 torr, and a net current of 17,000 A, we estimated $\omega/\nu \approx 0.05$. For 0.1 torr, we find a decay time of ~ 200 nsec, and peak currents of ~ 50 kA giving $\omega/\nu > 1$. We see, therefore, that tensor conductivity effects must be included if we are to fully understand the behavior in the 0.1-torr range.

Focusing on the 1-torr range, we can relate the plasma current at a given radius to the rate of change of the flux between that radius and that of the surrounding conductor, r_b, by the following:

$$\frac{\left(\vec{J}_{pl}\right)_z}{\sigma} = E_z = \frac{-\partial}{\partial t} \int_r^{r_b} B_\theta(r')\, dr'$$

With Ampere's law including the displacement current, we find that

$$B_\theta(r') = \frac{\mu_o}{2\pi r'} \int_o^{r'} \left(\left(\vec{J}_{pr}\right)_z + \left(\vec{J}_{pl}\right)_z + \varepsilon_o \frac{\partial \left(\vec{E}\right)_z}{\partial t} \right) 2\pi\, r''dr''$$

If we consider times which are long compared with the relaxation time, $\tau = \varepsilon_o/\sigma$, we than have a diffusion dominated problem described by:

$$\frac{\left(\vec{J}_{pl}\right)_z}{\mu_o \sigma} = -\left\{ \frac{\partial \left(\vec{J}_{pr}\right)_z}{\partial t} \frac{\left(r_b^2 - r^2\right)}{4} + \int_r^{r_b} \frac{1}{r'} \left[\int_o^{r'} \frac{\partial \left(\vec{J}_{pl}\right)_z}{\partial t} r''dr'' \right] dr' \right\} \qquad (1)$$

If the conductivity is a function of time and radius, a solution for J_{pl} would involve a nonlinear problem.

If, on the other hand, we take $\sigma = 0$ for $0 < t < t_1$, where t_1 is the breakdown time, and = constant independent of time and radius for $t > t_1$, we see some features of the solution.

Although (1) has not been solved, a zero order approximation can be generated for $r/r_b << 1$. Expanding the z component of the plasma current in a Taylor series,

$$J_{pl} = J^o_{pl}(t) + \varepsilon\, J^1_{pl}(t) + \varepsilon^2\, J^2_{pl}(t) + \ldots., \quad \varepsilon = r/r_b$$

we find:

$$J^o_{pl} + kA\sigma \frac{\partial J^o_{pl}}{\partial t} = - kA\sigma \frac{\partial J_{pr}}{\partial t} \qquad (2)$$

where $A = \pi r_b^2$, and $k = 10^{-7}$ in mks units.

If $\partial J/_{pr}/\partial t$ is know, Equation (2) can be solved for J^o_{pl}. To exemplify the behavior of the solution let us take a simplified functional form for the primary current. This is shown in Figure 19 as I_{pr} approximate where $I_{pr} = J_{pr}(A)$. The solution is then given by:

$$(-J_{pl}) = 0 \qquad 0 < t < t_1$$

$$(-J_{pl}) = a_1\, kA\sigma \left[1 - e^{-(t-t_1)/kA\sigma}\right] \qquad t_1 < t < t_2$$

$$(-J_{pl}) = a_2\, kA\sigma\, e^{-(t-t_2)/kA\sigma} \qquad t_2 < t < t_3$$

$$(-J_{pl}) = kA\sigma \left[a_3 - a_4\left(1 - e^{-(t-t_3)/kA\sigma}\right)\right] \qquad t_3 < t < t_4$$

$$(-J_{pl}) = a_5\, kA\sigma\, e^{-(t-t_4)/kA\sigma} \qquad t > t_4$$

Measured primary and net current (averaged over the beam area) at 0.75 torr, in addition to results of the above calculation, using $kA\sigma$ = 200 nsec and t_1 = 5 nsec are also shown in Figure 19. The results of the above calculation using t_1 = 0 and t_1 = 9 nsec appear in Figure 20, further demonstrating the importance of breakdown time. The excellent agreement between the measured average net current and that calculated for the center of the beam may be fortuitious; further measurements over a wider range of conditions are justified.

Early results imply, however, that a diffusion dominated problem with conductivity relatively constant in time, except for a rapid change at breakdown, provides a valid description of many essential features of current neutralization.

Measurements of net current at 10, 51.4, and 154 cm from the anode are shown in Figure 21. Calculating (ν/γ) net using the voltage monitor to give $(\beta\gamma)$ as a function of time, we find that $(\nu/\gamma)_{net}$ increases from approximately 0.5 early in the pulse to a value of approximately 1.0 at a later time. Time of flight measurements discussed in the following section show a value of longitudinal drift velocity consistent with these values of $(\nu/\gamma)_{net}$.

C. BEAM TIME OF FLIGHT

1. General Discussion

The propagation velocities of different portions of the beam were determined with scintillator photodiode detection of the bremsstrahlung produced when the beam strikes a tantalum target placed at the end of 1-1/4-in.-diam guide pipes. The bremsstrahlung output reflected the periodic oscillations in

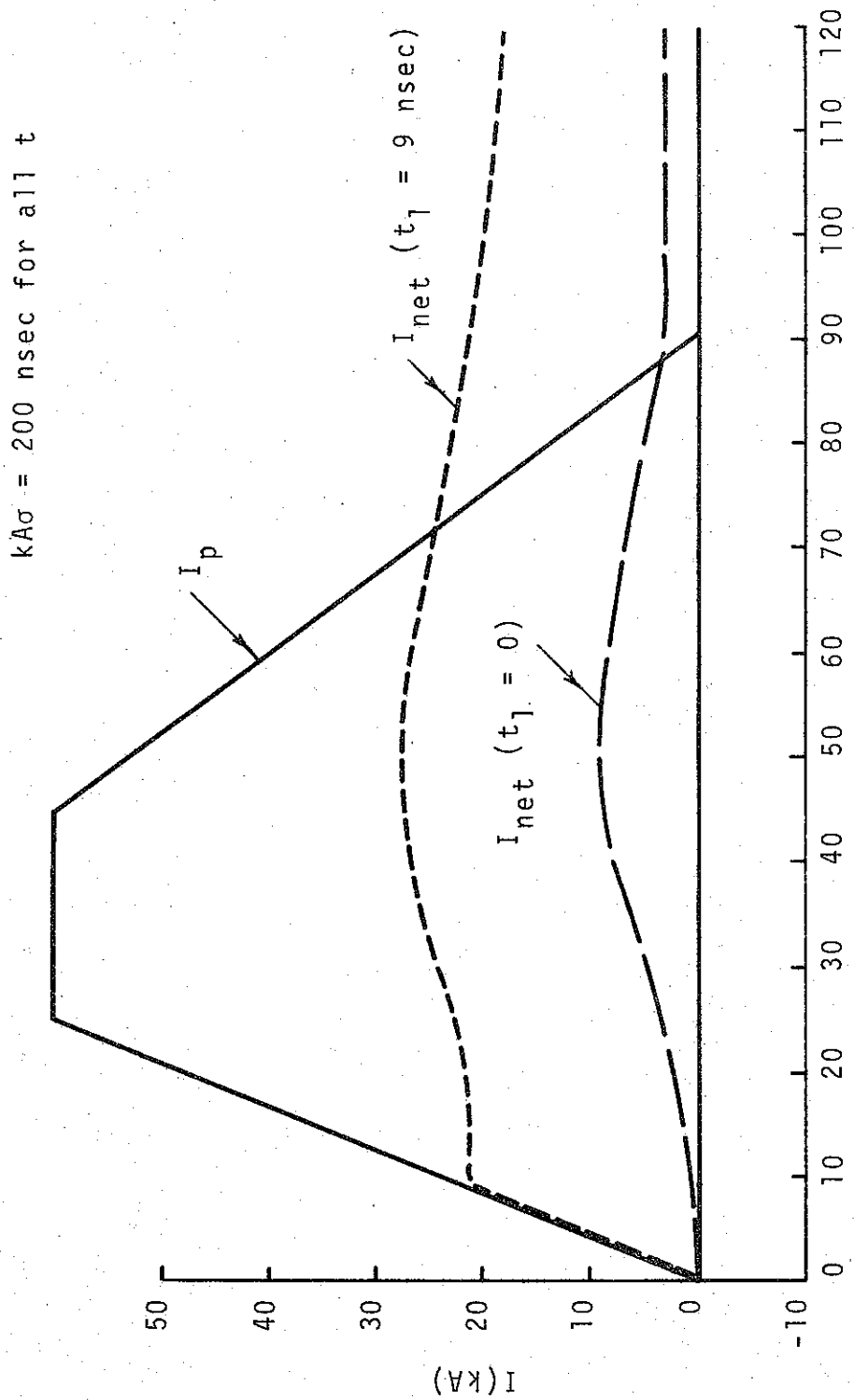

FIGURE 20. CALCULATED NET CURRENT (t_1 = 0 nsec, t_1 = 9 nsec)

3791

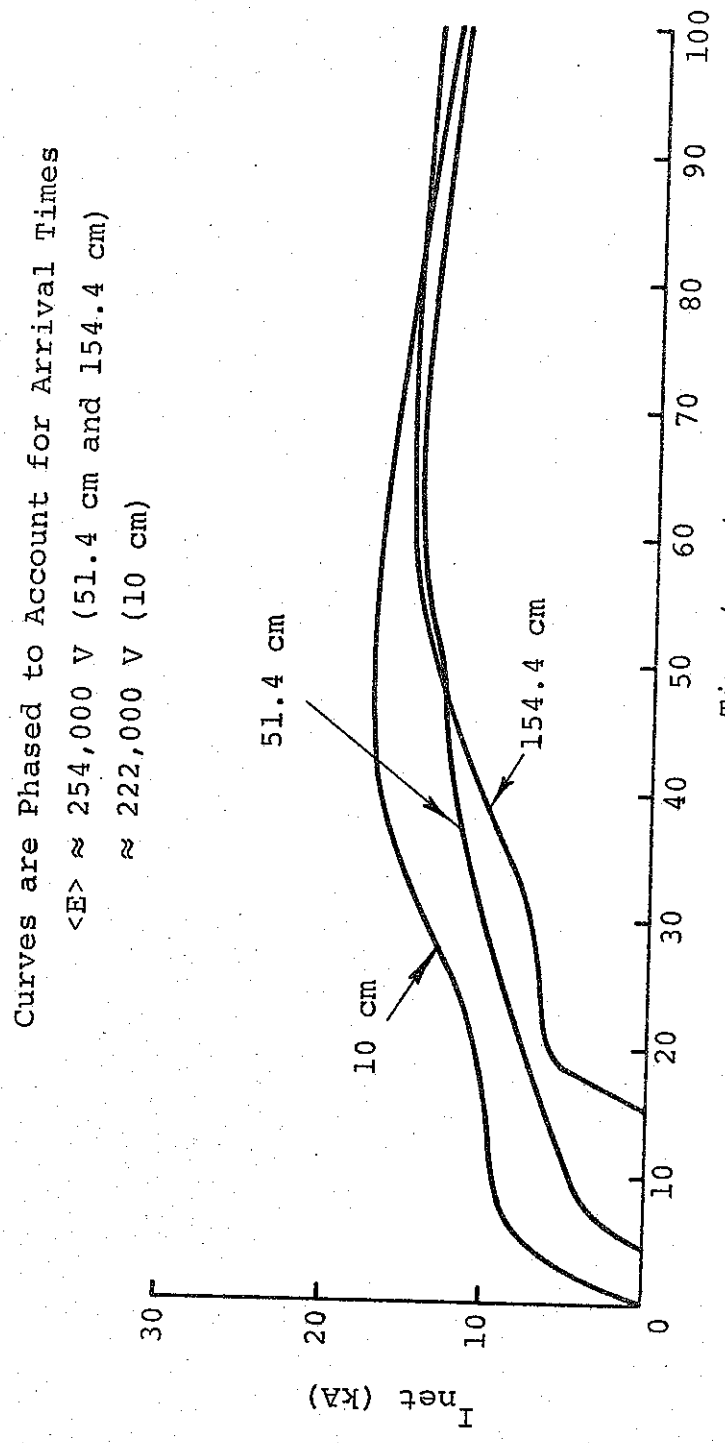

FIGURE 21. NET CURRENT VERSUS TIME IN 1-1/4-in. PIPE AT 0.75 torr AT 10, 51.4, and 154.4 cm

the voltage and current, thereby identifying different portions of the beam. (Figure 22 shows this structure in the bremsstrahlung output from a 0.0005-in. tantalum foil at the anode.) The photodiode output was monitored on an oscilloscope. The $\partial B/\partial t$ signal induced by the beam current rise at the anode triggered the monitor. In this way the absolute initiation time for the bremsstrahlung pulse could be measured.

Figure 22 presents a typical set of photodiode outputs at four different longitudinal distances from the anode. Zero time is indicated on each trace, and the individual peaks are identified by numbers 1 through 4. Velocities of the beam front and the four distinct bremsstrahlung peaks are most clearly illustrated by plots of absolute arrival time versus longitudinal distance. Figure 23 presents these data at six different pressures--0.1, 0.3, 0.5, 0.75, 1.0, and 2.0 torr.

It is evident from Figure 23 that the beam front velocity varies with pressure and appears to decrease monotonically with longitudinal distance. The beam front arrival time versus distance is plotted for all the above pressures in Figure 24. At 3 m the beam front velocity increases when pressure increases from 0.1 to 1.0 torr. The 2.0 torr data is identical within the limits of error to that observed at 1.0 torr for distances < 3 m. At 4 m, the front velocity at 2.0 torr appears smaller. With the aid of our net current measurements, it was possible to suggest a mechanism for the decrease in beam front velocity with distance. This is discussed in the next subsection.

Another interesting observation, the bulk of the beam appears to be traveling at a longitudinal velocity higher than that of the beam front. Diode voltage monitor records were used to determine β for the various bremsstrahlung peaks. These data were then

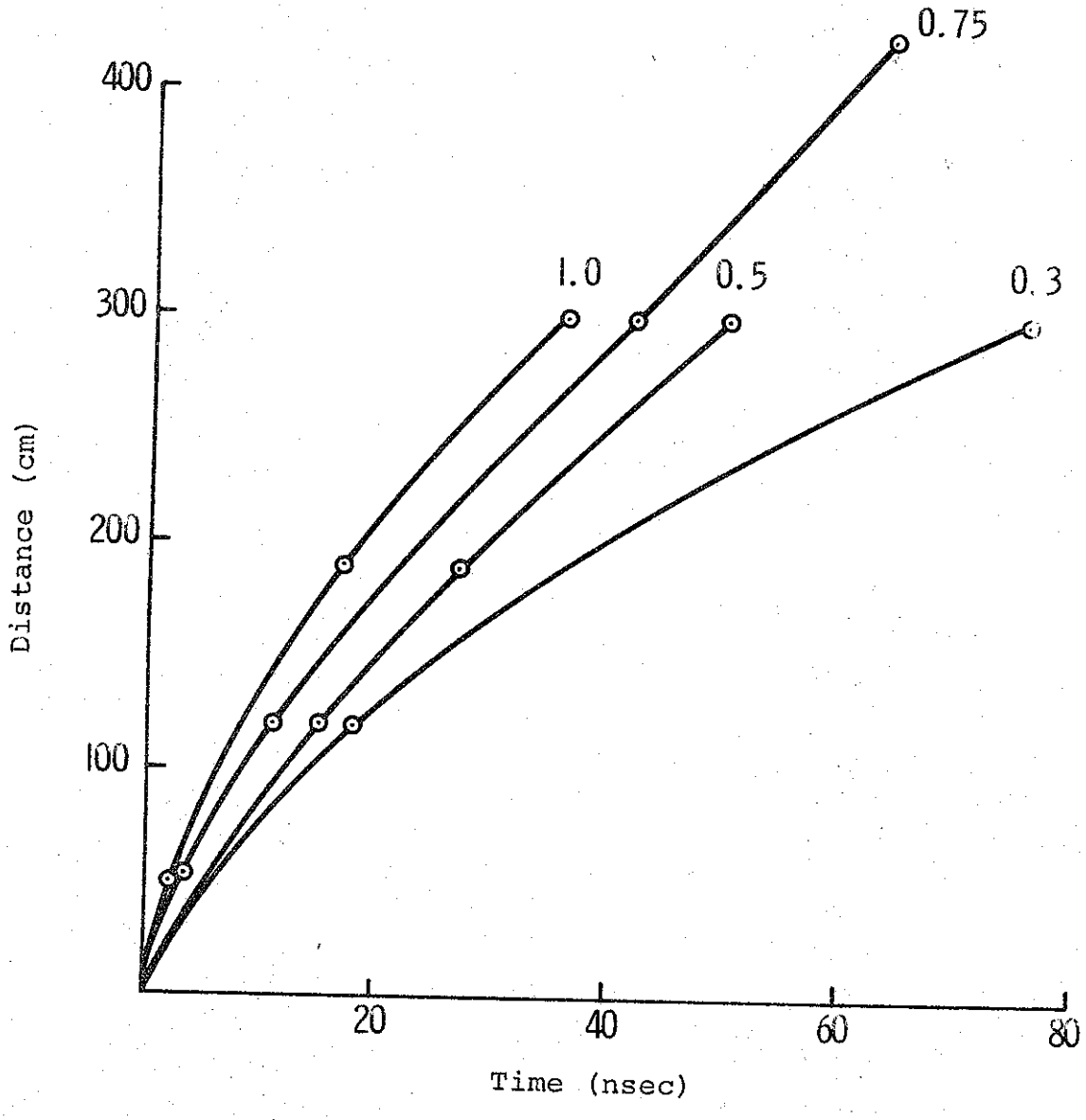

FIGURE 24. BEAM FRONT TIME OF FLIGHT

compared with β_L, the ratio of the longitudinal drift velocity to the speed of light. This comparison indicates a trend for β_L/β to decrease with distance into the beam (i.e., β_L/β for the third peak > β_L/β for fourth). Net current measurements show that I_{net} increases between the time of the first and the fourth peaks, which indicates a correlation between large net currents and larger relative transverse velocities ($\beta^2 = \beta_L{}^2 + \beta_T{}^2$). It was found that for most pressures studied $\beta_L/\beta \approx 0.8$ for the second, $\beta_L/\beta \approx 0.73$ for the third, and $\beta_L/\beta \approx 0.7$ for the fourth peak. A notable exception occurred at 0.5 torr where $\beta_L/\beta \approx 0.4$ for the fourth peak. It should also be noted that the peak velocities were determined for relatively large transport distances (up to 3-4 m); net current measurements at these distances suggest $(\nu/\gamma)_{net} \leq 1$ for all pressures at distances ≥ 0.5 m. Thus, it is not unreasonable to expect little variation in β_L/β with varying pressure. The relatively low velocity of the fourth peak at 0.5 torr has not yet been explained, but more complete net current measurements may explain this irregularity.

2. Beam Front Velocity

One can obtain a zero order approximation for the electric field and estimate the work done on electrons at the beam front. From Equation (1) we find that for $r \approx 0$:

$$E_z = 10^{-7} \left(\frac{\partial J_{net}}{\partial t} \right) \pi \, r_b{}^2$$

As above, we use the measured average net current over the beam area to estimate E_z. For 0.75 torr and $\langle E \rangle \approx 230$ keV, Rogowski coil measurements at 10, 51.4, and 151 cm indicate that $\partial I_{net}/\partial t$ at the beam front does not change with distance and is equal to 1.6×10^{12} A/sec. This gives $E_z = 1.6 \times 10^5$ V/m. It is clear that fields of this order must have an important effect on the

electrons which begin their life at the anode within the time required for breakdown (~ 5 nsec for air at 0.75 torr). Also, after the front has traveled 1 to 2 m, the region near the front is being filled with electrons which have been traveling in a region of reduced electric field. Work is continually being done on new energetic electrons which replenish those lost by radial motion to the walls.

The model of breakdown described above indicates that the length of this region of large electric field at the beam front should increase as the pressure is decreased from 1.0 to 0.1 torr. Since the energetic electrons must pass through this region to reach the front, a larger beam front velocity for higher pressures is expected and observed.

One can speculate on the nature of the beam front region and on the degree to which electrons "pile up" before they can be lost to the walls. Recent measurements at Ion Physics Corporation (Reference 4) indicate a collective ion acceleration mechanism in high ν/γ beams, perhaps the result of a bunching of negative space charge at the beam front. If ions can be trapped for only a short time in a space charge potential well created by the bunching of electrons, then a fraction of the beam front velocity can be achieved.

A solution to the electrodynamic portion of the beam plasma interaction, performed by Sidney Putnam under this contract, supports the possibility of such an ion acceleration mechanism (Reference 5). John Wachtel (Reference 6) suggests another mechanism in terms of the work done on a test ion in a charge-neutralized beam by collective coherent oscillations of the remaining ions. Since one model allows for acceleration only near the beam front and

the other predicts energetic ions produced throughout the beam pulse, time-resolved ion detection measurements should provide insight into the nature of this mechanism.

Measurements with approximately 200-keV, 200-kA beams are planned to determine if energetic ions are being generated. We have indicated the presence of transverse energy within the beam, and some energy loss is clearly occurring at the beam front. Recent energy transport measurements which we hope to correlate with our observations of beam timing and net current are discussed in the following section.

D. TRANSPORT EFFICIENCY

Reference 1 indicates that beams can be transported in pipes with an e-folding distance of approximately 250 cm at pressures in the 0.5- to 1.0-torr range (Figure 48, Reference 1). Recent data on beam timing in a 1-1/4-in.-diam pipe demonstrated that the energy loss due to slowing down of electrons at the beam front was a minimum at 1.0 torr (highest velocity front). The net current data shown in Figure 15 also indicates a minimum loss at 0.75 to 1.0 torr.

To relate these observations to calculations of energy transport, we repeated our measurements at more carefully controlled pressures with data collected at 0.3, 0.5, 0.75, and 1.0 torr. The data clearly shows that at distances $\gtrsim$ 100 cm energy is most efficiently transported at 0.75 torr. An e-folding distance, λ, of 243 cm was determined for 0.75 torr and values of $\lambda \approx 180$ cm were found for both 0.5 and 1.0 torr (see Figure 25 and 26).

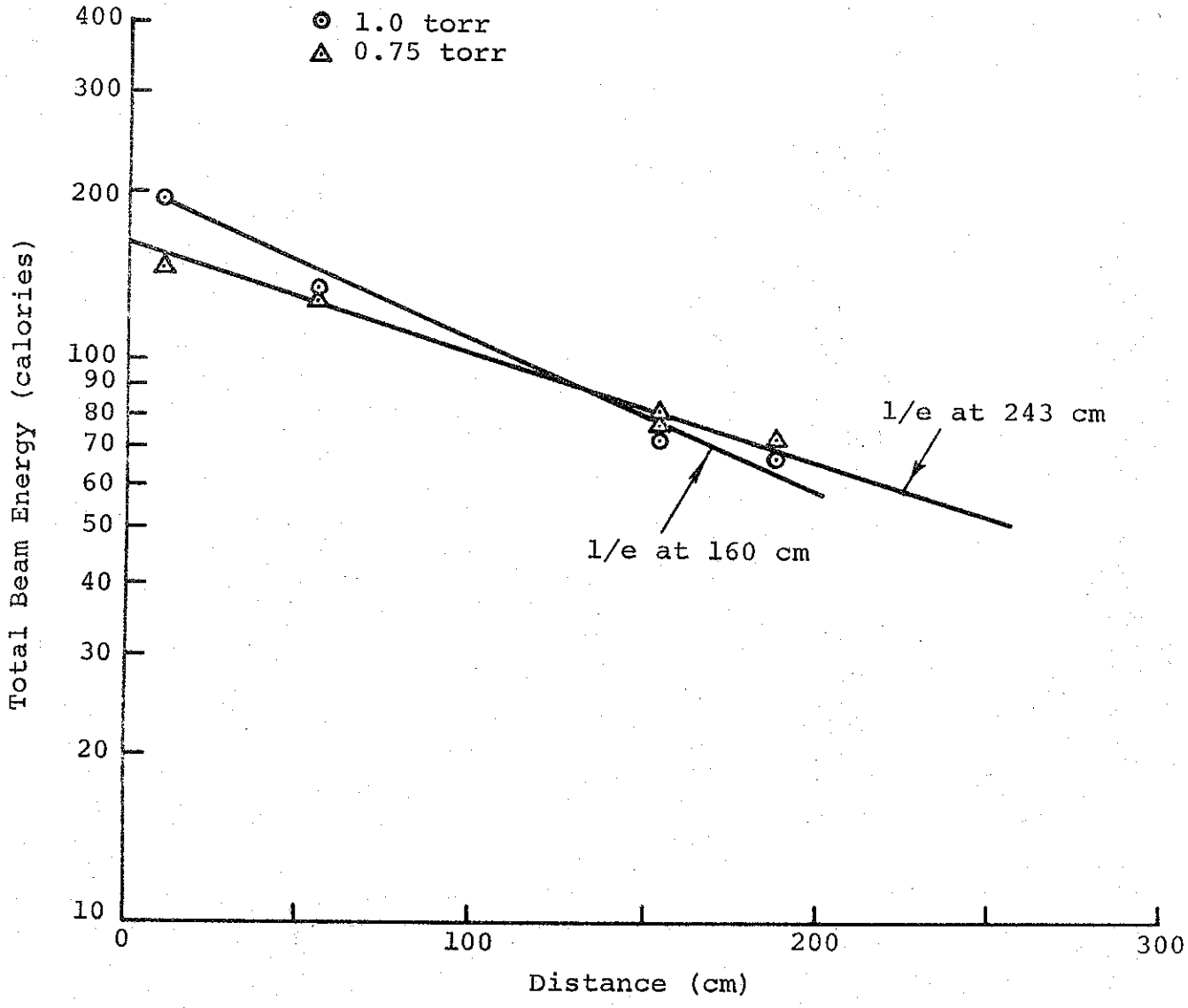

FIGURE 25. TOTAL CALORIES VERSUS PATH LENGTH IN 1-1/4-in. PIPE (0.75 AND 1.0 torr ~ 250 keV)

5804

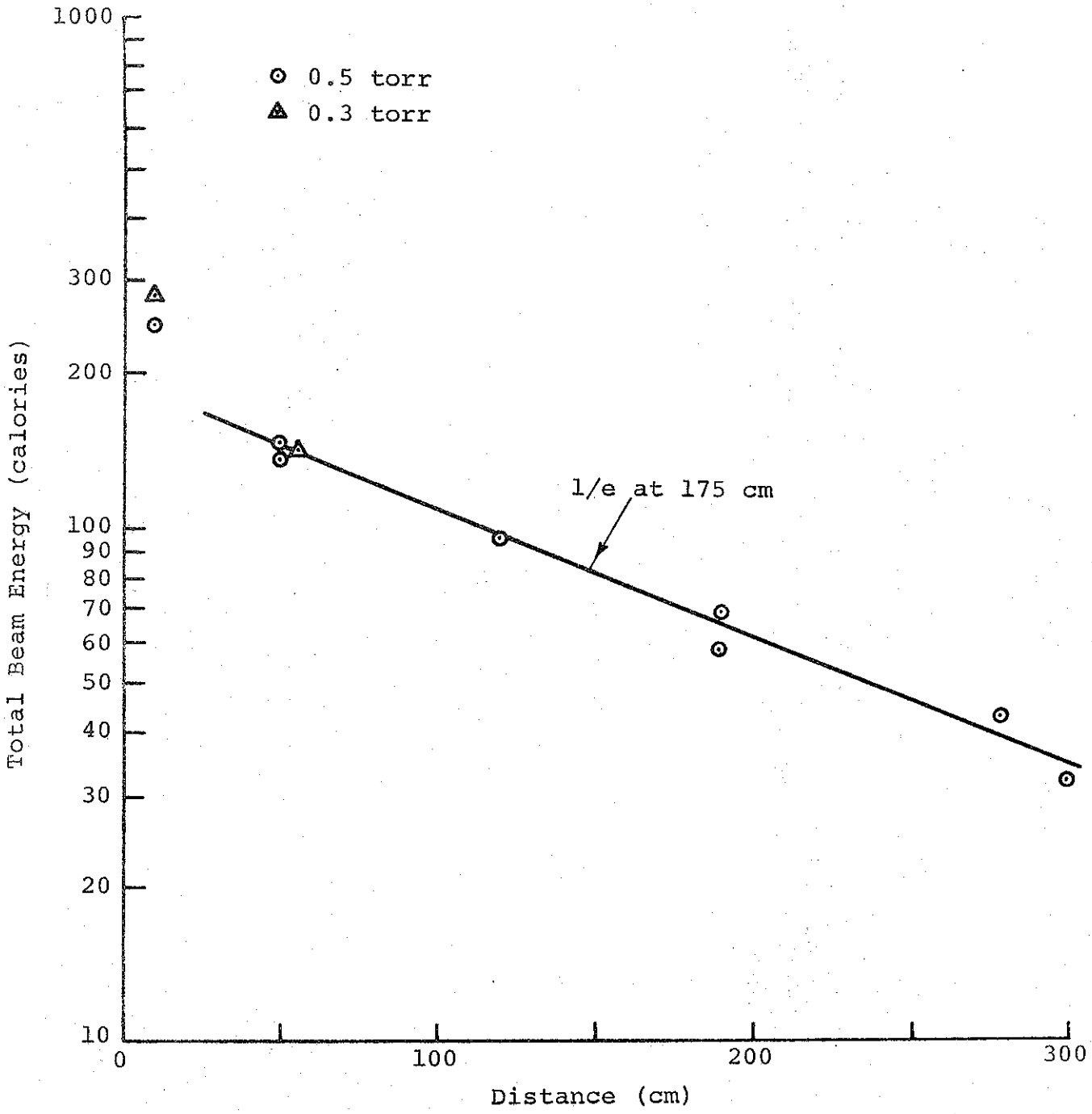

FIGURE 26. TOTAL CALORIES VERSUS PATH LENGTH IN 1-1/4-in. PIPE (0.5 and 0.3 torr ~ 350 keV)

5805

These measurements also revealed that initial total energy (extrapolating data back to x = 0) is greater at lower pressures, where higher net currents were observed. This relationship implies that the energy loss over initial short pipe lengths is governed by the guiding and focusing properties of the pipe. At longer distances, the higher longitudinal electric field over a greater portion of the beam, and the larger transverse velocites in the higher current region near the front contribute to energy loss. As a result, the optimum transport pressure depends on the transport length. Since the beam timing measurements indicate a roughly equal amount of transverse energy at distances greater than approximately 100 cm for all pressures, we conclude that energy loss associated with the beam front must dominate.

If we assume the beam energy loss is restricted to the beam front, the estimate of energy loss is far lower than that observed. As a result, we are unable to provide an explanation consistent with our observations of the experimental energy decay. It is hoped that net and primary current measurements at longer distances will clarify this observation.

E. TRANSMISSION FOIL MEASUREMENTS

The experiments discussed above suggest the existence of transverse components of electron velocity at pressures where (v/γ) net is ≈ 1. To verify this hypothesis, we conducted Faraday cup measurements of current transmission through metallic foils of various thicknesses placed at the end of a short metallic guide cone or a tube. The electron energy was determined by the diode voltage monitor; the purpose of this experiment was to observe changes in the electron transmission due to a non-zero mean angle of incidence at the transmission foil. The assumption

that the electron energy is not changed by propagation in a longitudinal electric field remains in question. However, net current measurements taken with a Rogowski coil indicate that, except for the short time before breakdown, (< 10 nsec), the net current time derivative is less than 10^{12} A/sec, so that $E_z \lesssim 10^3$ V/cm. As a result, we expect a negligible change in electron energy for pipe lengths ≤ 10 cm.

To estimate the average electron angle incident on the filter, we used a Monte Carlo electron transport code to determine features of electron deposition. Fractional transmission and deposition profiles as a function of filter thickness for several assumed average angles of incidence $\overline{\theta}$ were obtained. Figure 27 shows the results of these measurements at the end of a 12-cm-long, 1-1/4-in.-diam pipe at pressures of 0.5 and 0.75 torr with superimposed calculations for 45 and 60 deg. There is evidence of angles in the 45- and 60-deg range and indications that the average angle is greater at 0.5 than 0.75 torr. Simultaneous measurements with a Rogowski coil at the tube exit gave peak net currents of 50 kA at 0.5 torr and 25 kA at 0.75 torr ($\langle E \rangle \approx 200$ keV) giving ν/γ_{net} of 3.0 and 1.5 respectively. Surprisingly, the correlation of average angle with ν/γ is identical with that predicted by extending Lawson's model beyond its range of validity

$$\tan \overline{\theta} \doteq \left[\frac{\langle \beta_T^2 \rangle}{\langle \beta_L \rangle^2}\right]^{1/2} \doteq (\nu/\gamma)_{net}^{1/2}$$

Lawson (Reference 7) has pointed out, however, that this condition can be derived independently of his original assumptions of almost paraxial trajectories if the transverse energy is interpreted in terms of a kinetic temperature. With such an interpretation,

one could expect beams of arbitrarily large values of $(\nu/\gamma)_{net}$ and a correspondingly large ratio of transverse to longitudinal energy. Our measurements indicate that such beams can exist over short distances, but that readjustment of the primary current occurs so as to reduce $(\nu/\gamma)_{net}$ to ~ 1 if the beam is propagated an appreciable distance. Further measurements should include initial values of primary current sufficiently low that $(\nu/\gamma)_{pr} < 1$ and a wider range of pressures to determine if the correlation discussed above has general validity.

F. BEAM MANIPULATION

Extending our investigation of metallic beam guides, we have studied: (1) beam splitting by a sharp edge metallic plane, transport of the split beam and its recombination; (2) injection of the beam into its own "wake" using a re-entrant guide configuration; and (3) the pressure and energy dependence of guide properties in metallic cones.

1. Beam Splitting

A 250-keV beam was injected (at 0.5 torr) into the metallic guide cone and beam splitter shown in Figure 28a. The cone exit area was equal to the cross-sectional area of the two 3/4-in.-diameter pipes. Total beam energy measurements on two consecutive shots, first at the cone exit and then at the ends of the beam splitter pipes, showed that of the 219 cal incident at the cone exit, 152 cal were transported through the two pipes (75.5 through one, and 76.5 through the other). We observed slight damage to the splitting plane which may explain the measured loss of approximately 30% of the beam energy in splitting and transport over the 20-cm length of pipe.

Similar successful experiments were performed with an array of four guide pipes shown in Figure 28c. It appears that beam division by metallic guide planes is an effective and reasonably efficient process. With indications of transverse energy components in the beams, the fact that beam splitters work at all implies a rapid readjustment of the beam to the new boundary conditions imposed by the sudden change in guide configuration.

Attempts were also made to recombine the separate beams generated by the dual beam splitter. First, two beams were injected into a single 3/4-in.-diam pipe using a "Y" shaped fitting. Initial measurements showed that only 40% of the energy injected into the "Y" was transported into the exit pipe. In a subsequent shot where the fitting was cut back to the plane at which the two pipes were joined (Figure 29a), the resulting combined beam spread into a large, low-fluence area with many residual higher fluence filaments. We suspect that space charge repulsion of the beam fronts is significant, but further study is required to determine if beams can be combined effectively.

2. Re-entrant guides

We attempted to inject an electron beam into its own channel with the re-entrant guide configurations shown in Figure 30. The re-entrant hoop with a solid outer guide wall appeared to be less lossy than the mesh pipe, but both configurations appeared too lossy for optimum reinjection. The scintillator photodiode output from the shot (Figure 30b) showed that breamsstrahlung production stops after 70 nsec, indicating that no large fraction of the beam made more than one circuit around the ring. By placing a calorimeter just to the right of the Rogowski coil (see Figure 30c), we determined that propagation past the discontinuity at the reinjection point caused a great deal of energy loss. Further investigations with other guide configurations are in progress.

3. Metallic Guide Cones

In DASA 2175 (Reference 1) it was reported that beam control at 0.5 torr by the use of metallic guide cones produces uniform fluence distributions over areas as large as 3 cm^2. Since that time, guide cones have been used during most applications experiments on the Model 730 Pulserad, and we have collected data at different energies and pressures that further document the properties of these guides.

Fluence uniformity over the cone exit area was investigated by pinhole photography of the bremsstrahlung produced with a tantalum target at the cone exit. The pinhole photographs in Figure 31 show a uniform density spot corresponding to the cone exit area. The elliptical shape of the spot is due to the positioning of the pinhole 30 deg off axis from the cone centerline. This evidence, the observations of uniform depth craters (Reference 1), and recently, the production of one-dimensional rear surface spall over the target area, strongly supports the existence of uniform fluence at the cone exit.

It is now also clear that the use of guide cones is not limited to electron beams of a lower mean energy ($\simeq$ 250 keV). With only small changes in the guide configuration (i.e., larger entrance diameters for higher energies because of weaker pinching in the A-K region before injection), we have produced uniform fluences over 3 cm^2 at 1-MeV electron energy. Several other tests have been successful at 500 and 750 keV. Changes in drift chamber pressure affected the magnitude of the fluence levels while preserving fluence uniformity in the 0.5- and 0.8-torr pressure range. (At 0.8 torr, the fluence was lower by about a factor of two.) Below 0.5 torr, the fluence levels increased at the expense of uniformity over the entire exit area; yet,

uniformity over much of the exit area was preserved. Near 1.0 torr the fluence distribution was marked by the appearance of a small, high-intensity filament on the beam axis.

Fine screen mesh cones, as well as the slotted cone shown in Figure 32, (Rogowski coil at the exit) were found to control the beam as well as solid wall guide cones. These special cones were designed to minimize the effect of anode debris on material response experiments.

SECTION IV

SUMMARY AND FUTURE PLANS

The major conclusions of this report relate to the observation of $(\nu/\gamma)_{net} \sim 1$ for beams transported in the 0.5 - 1.0-torr range, and definite evidence of beam electron trajectories with non-negligible components of transverse velocity. Time of flight, deposition profile, and transmission measurements indicate that

$$\frac{\langle \beta t^2 \rangle}{\langle \beta_L \rangle^2} \sim 1,$$

giving consistent agreement with an extension of Lawson's model or an interpretation of the beam behaving as a plasma stream. Time-dependent measurements of net and primary current have been correlated with a diffusion dominated model of current neutralization which depends on the time dependence of the primary current and two background gas parameters--(1) avalanche breakdown time, and (2) plasma conductivity. Measurements of energy transport were compared with beam front "erosion" rate, and primary electron energy degradation in the inductively induced electric field near the beam front was suggested as the major loss mechanism.

To test many of the features of this model of high ν/γ beam transport it is suggested that pre-ionization of the background gas can effectively provide a zero value of breakdown time and, if our model is correct, lower values of net current, energy loss rate, and β_T. The other parameter of considerable importance is the primary current which should be varied through both considerably higher and lower ranges. The 1-2 MA, 100-keV Mylar and copper sheet strip line pulser now under development (Contract DASA 01-69-C-0016) should provide an ample test for many of these concepts.

Experiments to be continued include net and primary current measurements at greater distances from the anode. In particular, we plan to measure net currents at as many as four distances, as well as the primary current at the end of the long guide pipe, on a single shot. In this way it will be possible to investigate the longitudinal dependence of net current at different pressures and independently measure the beam front arrival time versus distance. The effect of varying both $(\nu/\gamma)_{primary}$ and the primary current will also be studied. By varying machine parameters it is possible to compare transport characteristics for (1) beams with equal mean electron energy but different primary currents, and (2) beams with equal currents but different mean electron energies. Other areas of investigation will include other reinjection techniques, preliminary ion detection experiments, and pre-ionization effects.

REFERENCES

1. G. Yonas and P. Spence, "Experimental Investigation of High ν/γ Electron Beam Transport," PIFR-106, DASA 2175, Physics International Company, San Leandro, California (October, 1968).

2. J. Creedon, "Pressure Dependence of the Pinched Electron Beam Mode," PIIR-16-67, Physics International Company, San Leandro, California (March, 1967).

3. P. Felsenthal and J. M. Proud, "Nanosecond-Pulse Breakdown in Gases," Phys. Rev. 139, A 1796 (September, 1965).

4. S. Graybill, "Particle and Spectroscopic Diagnostics of Beam Plasma Systems," Conference on Intense Relativistic Electron Beams, Cornell University, January, 1969).

5. S. Putnam, "Experimental and Theoretical Electron Beam Research," PIQR-105-3, Physics International Company, San Leandro, California (February, 1969).

6. J. M. Wachtell, "Collective Acceleration of Ions by Intense Electron Beams," Conference on Relativistic Electron Beams, Cornell University, (January, 1969).

7. J. D. Lawson, "On the Classification of Electron Streams," J. Nucl. Energy, Part C: Plasma Physics, 1, 31-35 (1959).